IMPROVING GEOSTATIONARY SATELLITE GPS POSITIONING ERROR USING DYNAMIC TWO-WAY TIME TRANSFER MEASUREMENTS

Capt. Benjamin Dainty, John Raquet, and Capt. Richard Beckman
Advanced Navigation Technology (ANT) Center
Air Force Institute of Technology
AFIT/ENG, 2950 Hobson Way, Wright-Patterson AFB, OH 45433, USA
E-mail: *John.Raquet@afit.edu*

Abstract

GPS signals can be used for positioning satellites in geostationary (GEO) orbits, but the performance in this case is poor, because very few pseudorange measurements are available at any given time. This paper describes a new method for improving geostationary satellite navigation accuracy by using dynamic Two-Way Time Transfer (TWTT) measurements. By directly measuring the clock error between the GPS satellite and the GPS receiver, TWTT allows meaningful information to be gathered when less than four GPS satellites are available. A simulation was developed in which satellites in GEO orbits with GPS receivers onboard generated a position with 1) GPS with a crystal clock, 2) GPS with an onboard atomic clock, 3) GPS with TWTT to a ground-based atomic clock, and 4) GPS with TWTT to a ground-based clock synchronized to GPS time. Bringing an atomic clock into the system (Cases 2 and 3) resulted in a 21-38% improvement in the 3-D RMS position accuracy over the standard GPS case (Case 1). However, using TWTT with a clocked slaved to GPS time resulted in a 60%-70% improvement in 3-D RMS positioning accuracy. This level of performance was obtained for TWTT measurement error standard deviations anywhere between 0.3 ns to 30 ns.

INTRODUCTION

Dynamic two-way time transfer (TWTT) has recently been demonstrated **[1,2]**, opening up the possibility of using TWTT measurements to improve GPS-based navigation solutions on moving platforms. Previous research has shown a 40% improvement in DGPS positioning accuracy when using TWTT to synchronize clocks between a network of GPS receivers **[3]**. Similar results can be found in **[4]**.

The main objective of this research was to examine the impact of adding dynamic TWTT measurements to GPS-based geostationary (GEO) satellite positioning. Using GPS to position satellites in GEO orbits can be a challenging task. Most of the L-band RF energy transmitted by the GPS satellites is aimed at the Earth, and only occasionally is a GEO satellite within the main beam of a GPS satellite, as shown in Figure 1. As a result, very few pseudorange measurements are typically available for positioning a GEO satellite. Figure 2 shows an example of the number of available GPS measurements for a GEO satellite over a 1-day period. From this plot, it is clear that having four satellites (which is required to obtain a full position/clock error solution) is a relatively rare occurrence for a GEO satellite. When fewer than four measurements are available, then the receiver clock error cannot be estimated, and receiver clock errors will affect the positioning solution.

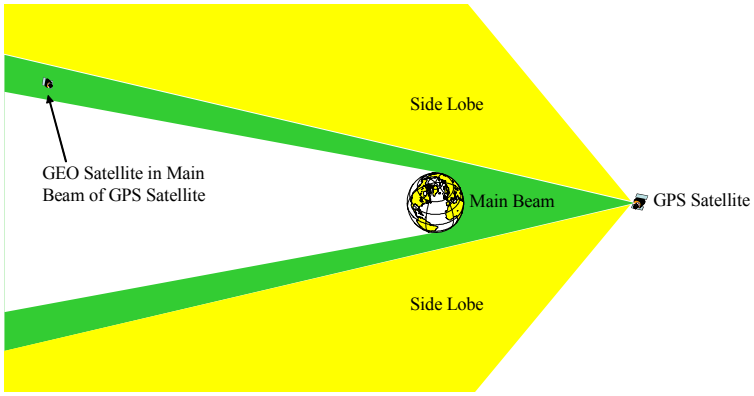

Figure 1. GPS/GEO satellite coverage geometry.

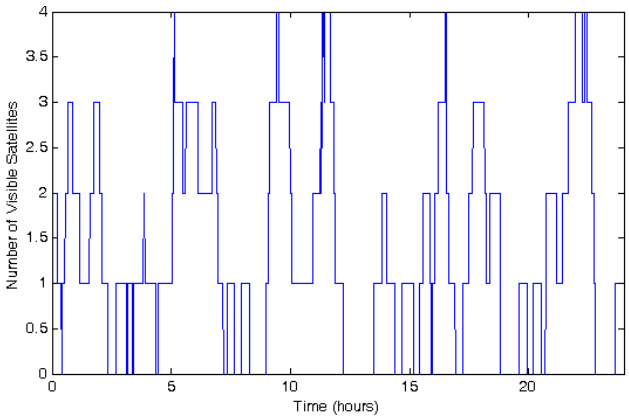

Figure 2. Example of the number of available pseudorange measurements for a standard GPS receiver in orbit on a GEO satellite.

The thought behind this research is that by using TWTT measurements to help constrain or measure the GPS receiver clock error, then the positioning solution should be improved for a GEO satellite. TWTT measurements should eliminate the need for a precise clock on the satellite, because it would only need a precise reference clock on the ground. Essentially, using TWTT with a highly accurate clock on the ground and a low-quality clock on the satellite would be comparable to putting a highly accurate clock on the satellite itself. Even better performance should be possible by using the TWTT system to directly measure the absolute GPS receiver clock error on the GEO satellite by synchronizing the GPS receiver clock to a clock slaved to GPS system time.

A simulation was developed in order to evaluate the effect of different ways to use TWTT measurements to improve positioning of GEO satellites. This paper describes the simulation and summarizes the key results obtained by running the simulation.

BACKGROUND

Two-Way Time Transfer (TWTT) is a technique in which signals are simultaneously exchanged between two users to measure their relative clock offsets. If the paths between the two users are reciprocal, the delays cancel and the difference between the two clocks is half the difference in time-interval counter readings **[5]**.

TWTT can be performed in both static and dynamic modes. Static TWTT uses two or more transceivers whose positions on Earth are held constant during the transmission and reception of the measurement signals. Dynamic TWTT is a more recent development that allows one or more of the transceivers to be moving **[1,2]**.

DYNAMIC TWTT

Dynamic TWTT is accomplished in the same fashion as static TWTT, with the exception that one or more of the receivers is moving. The moving receiver(s) introduce motion-related errors that are not present in the static case. A dynamic TWTT configuration is illustrated in Figure 3.

Not all of the cancellations that applied to the static TWTT case transfer to the dynamic case. For the dynamic TWTT scenario in Figure 3, it can be assumed that $d_{AS} \approx d_{SA}$, since the geostationary satellite has no relative motion with respect to the earth station and the path length does not change. This replicates the situation in the static case. Unlike the static case, $d_{SB} \neq d_{BS}$ for the dynamic case, since the mobile platform has moved during the transmission of signals, causing the transmit and receive path lengths to be different between the geostationary satellite and mobile platform. Because the mobile platform is in motion, the Sagnac effect will also vary and produces a time-dependent value.

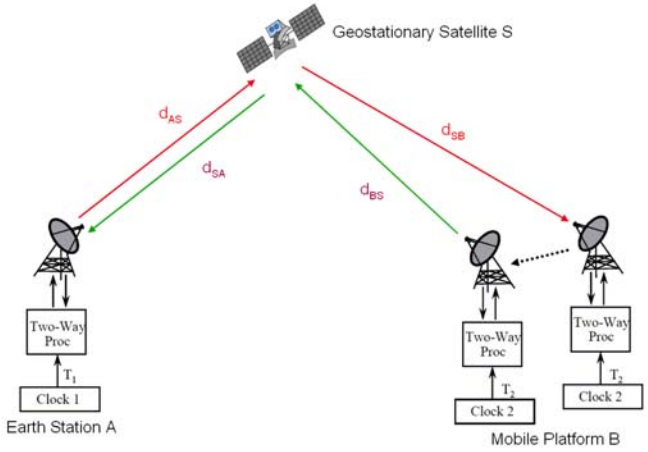

Figure 3. Dynamic TWTT using a satellite **[2]**.

Taking all this into account, the time differenced measurement for dynamic TWTT becomes:

$$A - B = \frac{1}{2}[R(A) - R(B) - \Delta PropDelay + S_{AB} - S_{BA}] \quad (1)$$

where

R(A) = time-interval counter reading for Station A
R(B) = time-interval counter reading for Station B
S_{AB} = Sagnac delay from Station A to Station B
S_{BA} = Sagnac delay from Station B to Station A
A = time of Clock A
B = time of Clock B
$\Delta PropDelay$ = change in propagation delay over measurement interval.

The $\Delta PropDelay$ term is a time-varying value that changes based on the relative motion of the mobile platform as well as how the velocity vector is projected onto the line of sight vector from the geostationary satellite. The Sagnac delay term ($S_{AB} - S_{BA}$) is also time-varying, changing based on the absolute position of the two receivers and the velocity vector projected onto the equatorial plane **[2]**.

METHODOLOGY

This research is based on a simulation created using MATLAB® and contains five main functions, seen in Figure 4. The *load_params* function involves collecting desired input parameters from the user. The *generate_truth* function uses the input parameters to create truth data that will simulate the environment that is being measured. The *generate_meas* function uses the truth data to generate pseudorange and TWTT measurements for a geostationary satellite. The *kalman* function inputs the generated measurements into a Kalman filter and predicts the state of the satellite at each epoch in the simulation. The *analyze_results* function takes the results of the Kalman filter and compares them to the truth data to determine the accuracy of the filter. Each of these functions will be briefly described in the sections that follow.

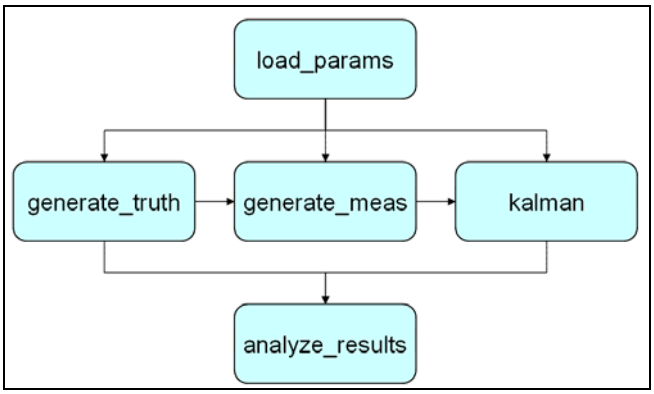

Figure 4. Simulation block diagram

PARAMETERS

The simulation begins by collecting all the desired input values for a host of variables that are used throughout the simulation. The essential parameters are:

- Initial ECI state for the geostationary satellite
- Simulation run time and time step interval (set to 1 day of simulation with measurements at 1-minute intervals)
- GPS satellite ephemeris date selection

- Clock type selection and clock model parameters
- Two-Way Time Transfer measurement accuracy
- Kalman filter parameters (noise values, etc.)
- Monte Carlo parameters (e.g., number of runs).

TRUTH MODEL

The truth model function is responsible for generating all data that will be considered as the absolute truth. There are three main operations that happen in this function: 1) propagation of the geostationary satellite state forward over a specified time interval, 2) calculation of the true GPS satellite position and clock at measurement times, and 3) clock error modeling.

GEO Satellite Propagation. Implementation of a simple Kalman filter propagates the GEO satellite state vector into the future. The initial state vector $\hat{\mathbf{x}}(t_0)$ is provided, along with an initial covariance matrix $\mathbf{P}(t_0)$ and a dynamics matrix $\mathbf{F}(t_0)$. The covariance matrix describes the accuracy of the state vector values and the dynamics matrix explains the motion of the state vector.

The GEO satellite state vector is comprised of three position and three velocity states, as shown in Equation (2). Note that the simulation is implemented within an Earth-centered inertial (ECI) frame, and the final results are later converted to an Earth-centered Earth-fixed (ECEF) frame for ease of presentation and understanding.

$$\mathbf{x} = \begin{bmatrix} X & Y & Z & \dot{X} & \dot{Y} & \dot{Z} \end{bmatrix}^T \tag{2}$$

The continuous truth model for propagating the GEO orbit is

$$\dot{\mathbf{x}}(t) = \mathbf{F}(t)\mathbf{x}(t) + \mathbf{w}(t) \tag{3}$$

where the process noise $\mathbf{w}(t)$ is described by

$$E\left[\mathbf{w}(t)\mathbf{w}(t')\right] = \mathbf{Q}(t)\delta(t-t') \tag{4}$$

The dynamics matrix $\mathbf{F}(t)$ describes two-body the motion of the GEO satellite, and is written in continuous form as:

$$\mathbf{F}(t) = \begin{bmatrix} 0 & 0 & 0 & 1 & 0 & 0 \\ 0 & 0 & 0 & 0 & 1 & 0 \\ 0 & 0 & 0 & 0 & 0 & 1 \\ -\frac{\mu}{r^3} & 0 & 0 & 0 & 0 & 0 \\ 0 & -\frac{\mu}{r^3} & 0 & 0 & 0 & 0 \\ 0 & 0 & -\frac{\mu}{r^3} & 0 & 0 & 0 \end{bmatrix} \tag{5}$$

where μ is the Earth's gravitational parameter and r is the current orbital radius of the satellite.

A real satellite orbit would include the effects of many perturbing forces, such as higher-order gravity terms, the effect of solar pressure, gravity effects from the moon and sun, etc. Many of these effects are well understood and could be modeled in a real system. These types of deterministic effects were not modeled within the simulation, because they would basically be added into the truth model and then removed in the filter model, having no significant impact. However, it is understood that in the real world, the filter model will not perfectly match the truth model. To accurately represent this effect within the simulation, a small amount of dynamics noise was added to the truth model through the matrix **Q**(*t*):

$$\mathbf{Q}(t) = \begin{bmatrix} 0 & 0 & 0 & 0 & 0 & 0 \\ 0 & 0 & 0 & 0 & 0 & 0 \\ 0 & 0 & 0 & 0 & 0 & 0 \\ 0 & 0 & 0 & \sigma_n^2 & 0 & 0 \\ 0 & 0 & 0 & 0 & \sigma_n^2 & 0 \\ 0 & 0 & 0 & 0 & 0 & \sigma_n^2 \end{bmatrix} \tag{6}$$

GPS Satellite True Position and Clock Calculation. After propagating the GEO satellite state vector forward in time over the entire simulation time interval, the truth model function then calculates the positions and clock states of each individual GPS satellite over the entire simulation time interval. The true GPS satellite position and clock errors were calculated using a precise ephemeris (.sp3) file. Later, within the estimation Kalman filter, the position and clock error are calculated using the broadcast ephemeris data for the same time period. This means that there is a realistic difference between the truth and the modeled satellite positions that is representative of a particular day in GPS history.

Clock Modeling. The simulation needed to model the receiver clock error in the GPS receiver in the GEO satellite, as well as in an atomic clock on the ground (used in one of the scenarios described in the results section). For this simulation, the clock errors were modeled using a clock model given in **[7]**.

The performance of atomic clocks was simulated using a three-state polynomial process driven by white noise. The discrete process model was implemented as:

$$\begin{bmatrix} x_1(t_{k+1}) \\ x_2(t_{k+1}) \\ x_3(t_{k+1}) \end{bmatrix} = \begin{bmatrix} 1 & \tau & \frac{1}{2}\tau^2 \\ 0 & 1 & \tau \\ 0 & 0 & 1 \end{bmatrix} \begin{bmatrix} x_1(t_k) \\ x_2(t_k) \\ x_3(t_k) \end{bmatrix} + \begin{bmatrix} w_1(k) \\ w_2(k) \\ w_3(k) \end{bmatrix} \tag{7}$$

where

$x_1(t_k)$ and $x_1(t_{k+1})$ = clock bias error at times t_k and t_{k+1}
$x_2(t_k)$ and $x_2(t_{k+1})$ = clock drift error at times t_k and t_{k+1}
$x_3(t_k)$ and $x_3(t_{k+1})$ = clock drift rate error at times t_k and t_{k+1}
$\tau = t_{k+1} - t_k$ = time interval
$w_1(k)$, $w_2(k)$, and $w_3(k)$ = white noises.

The clocks cannot be modeled deterministically because of their stochastic nature. Instead, the performance of the random walk noise values (w_1, w_2, w_3) is modeled and the characteristic Allan variance curves of the atomic frequency standards are matched **[6]**. The statistics of the random walk

noise values are determined by the values of the variance continuous process noise power spectral densities (q_1, q_2, q_3) of $\mathbf{Q_d}$ in Equation (8).

$$\mathbf{Q_d}(\tau) = E\left[w(k)w(k)^{\mathrm{T}}\right] = \begin{bmatrix} q_1\tau + \frac{1}{2}q_2\tau^3 + \frac{1}{20}q_3\tau^5 & \frac{1}{2}q_2\tau^2 + \frac{1}{8}q_3\tau^4 & \frac{1}{6}q_3\tau^3 \\ \frac{1}{2}q_2\tau^2 + \frac{1}{8}q_3\tau^4 & q_2\tau + \frac{1}{3}q_3\tau^3 & \frac{1}{2}q_3\tau^2 \\ \frac{1}{6}q_3\tau^2 & \frac{1}{2}q_3\tau^2 & q_3\tau \end{bmatrix} \tag{8}$$

The results given later use both atomic (rubidium) clocks and ovenized crystal clocks (representative of a good crystal clock that would be used in a typical spaceborne GPS receiver). The q values for a spaceborne rubidium clock for this simulation were chosen by leveraging research conducted in the Clock Improvement Initiative **[7]** and are displayed in Table 1. The ovenized crystal clock parameters are obtained from **[6]**. To calculate a clock's three-state random process in the simulation, initial clock bias, drift, and drift rate values are selected from Table 1 and then propagated using Equation (7). The $\mathbf{Q_d}$ from Equation (8) was used to generate properly correlated w_1, w_2, and w_3 terms using a U-D factorization technique.

Table 1. Process noise values for simulated clocks.

	Rubidium Clock	**Ovenized Crystal Clock**
q_1 **(bias)**	1.11×10^{-22} s^2/s	1.6×10^{-21} s^2/s
q_2 **(drift)**	2.22×10^{-32} s^2/s^3	3.2×10^{-21} s^2/s^3
q_3 **(drift rate)**	6.66×10^{-45} s^2/s^5	0 s^2/s^5

GENERATED MEASUREMENTS

The measurement generation function is responsible for creating pseudorange measurements by using the information supplied by the truth generation function. Pseudorange values are normalized range measurements with the addition of errors due to pseudorange measurement noise, GPS satellite clock bias, and receiver clock bias. The pseudorange equation is:

$$\rho = \sqrt{(x^{sat} - x_{rec})^2 + (y^{sat} - y_{rec})^2 + (z^{sat} - z_{rec})^2} + c\delta t_{rec} - c\delta t^{sat} + \upsilon_{PR} \tag{9}$$

where

$x^{sat}, y^{sat}, z^{sat}$ = true ECEF position of the satellite (m)

$x_{rec}, y_{rec}, z_{rec}$ = true ECEF position of the receiver (m)

δt_{rec} = receiver clock bias (s)

δt^{sat} = satellite clock bias (s)

υ_{PR} = pseudorange error (m)

c = speed of light (m/s).

An important part of the GPS measurement model is determining exactly which GPS satellites are "visible" to the GEO GPS receiver at any point in time. Visibility is determined by a combination of received signal strength and a model of GPS receiver sensitivity.

RECEIVED SIGNAL STRENGTH

To determine the strength of the GPS signal that is received by the GEO satellite, the satellite nadir look angles are needed. If the GEO satellite and GPS satellite positions are known, simple vector math will produce the angles θ and α (referenced in Figure 5), which are the GPS satellite look angle and GEO satellite look angle, respectively. The calculated look angles are then used with antenna gain pattern information to determine the received signal strength. Additionally, any signal that passed within 400 km of the surface of the Earth was deemed unavailable due to atmospheric effects.

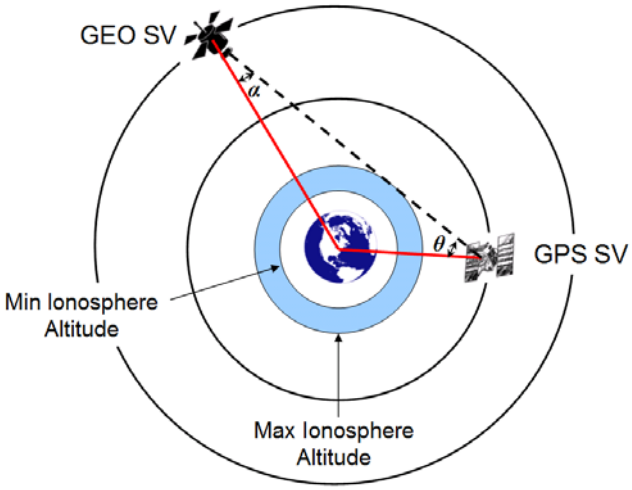

Figure 5. GPS measurement geometry.

The total received signal power can be calculated according to **[8]**:

$$P_s = \frac{P_T G_T G_R}{4\pi R^2} \frac{\lambda^2}{4\pi} \tag{10}$$

where

P_s = received signal power (watts)
P_T = signal power at transmit antenna
G_T = transmit antenna gain
G_R = receive antenna gain
R = distance between transmit and receive antennas
λ = signal wavelength (GPS L1 wavelength $\approx$ 5.255 m).

The resulting value is the signal power at the exit of the receiver antenna. A typical transmit (GPS satellite) antenna gain pattern was obtained from **[9]**. The GEO satellite receiver was modeled using the

gain pattern from a patch antenna that flew aboard the Falcon Gold experiment from the Air Force Academy **[10]**. This particular antenna is representative of hardware that has flown on previous satellites.

Once the total receive signal power was determined, a C/N_0 value was calculated by dividing by (or subtracting, if working in dB) a noise power density. This simulation uses a standard N_0 value of 202 decibel-watts **[8]**.

GPS Receiver Model. Once the received signal strength has been calculated, the pseudorange measurement noise error can be established through the use of a GPS receiver model. Fundamentally, the C/N_0 value defines whether or not a pseudorange measurement is available, and if it is, what the measurement noise would be.

Figure 6 shows the receiver models used in this simulation. The best performing receiver (labeled "High +") is derived from data obtained in **[11]**, and it is essentially an optimal receiver which performs better than most real receivers. Similar C/N_0 data is located in **[12]**. For each simulated receiver model, the point at which the line ends at the left represents the minimum C/N_0 value that will still yield a pseudorange measurement.

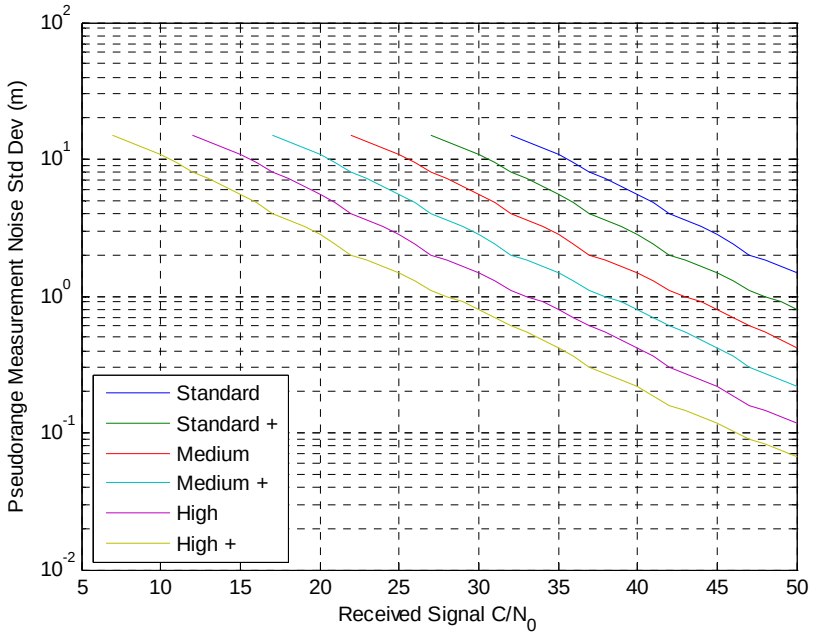

Figure 6. Simulated receiver models.

TWO-WAY TIME TRANSFER MEASUREMENTS

The Two-Way Time Transfer measurements in this simulation do not include Sagnac error or motion related errors, since they are largely deterministic and can be removed. The simulation could add the errors and then remove them, but this would be a wasted step that would only increase computational cost and would have no added value. For simplicity, this simulation assumes that the propagation delays will cancel as in the static TWTT case. The resulting TWTT measurement equation is:

$$\begin{aligned}\Delta T &= \tfrac{1}{2}\left[TIC(GEO) - TIC(REF)\right] + \upsilon_{TWTT} \\ &= \tfrac{1}{2}\left[2c\delta t_{GEO} - 2c\delta t_{REF}\right] + \upsilon_{TWTT} \\ &= c\delta t_{GEO} - c\delta t_{REF} + \upsilon_{TWTT}\end{aligned} \tag{11}$$

where

δt_{GEO} = GEO satellite clock error

δt_{REF} = reference clock error

υ_{TWTT} = TWTT measurement error

c = speed of light.

TWTT measurements are given to the Kalman filter along with the pseudoranges for measurement incorporation. The TWTT measurement noise standard deviation values used in this simulation are 10, 3, 0.3, 0.03, and 0.003 meters. (Units of meters rather than seconds are used because the system is ultimately designed to navigate. Dividing these values by the speed of light would give the values in seconds.)

KALMAN FILTER

A Kalman filter was chosen over a least-squares batch filter, since it allows for the use of new measurement data as they become available and easily models stochastic processes, such as clock errors. The Kalman filter has several initial values that govern the estimation algorithm. The filter must know the accuracy level of the incoming measurements and how much to trust in their positioning information, as well as the amount of process noise in the system.

The first thing needed by the Kalman filter is an initial state, including position, velocity, and clock error. These initial values are generated by adding the Gaussian random errors shown in Table 2 to the truth data. The state vector is defined as:

$$\hat{\mathbf{x}} = \begin{bmatrix} X & Y & Z & \dot{X} & \dot{Y} & \dot{Z} & c\delta t_{GEO} & c\delta \dot{t}_{GEO} & c\delta t_{ref} & c\delta \dot{t}_{ref} \end{bmatrix}^{\mathrm{T}} \tag{12}$$

where

X, Y, Z = GEO satellite position components

$\dot{X}, \dot{Y}, \dot{Z}$ = GEO satellite velocity components

δt_{GEO} and $\delta \dot{t}_{GEO}$ = GEO satellite clock bias and clock drift

δt_{ref} and $\delta \dot{t}_{ref}$ = TWTT reference clock bias and clock drift

c = speed of light.

Table 2. Initial state error standard deviation values.

Initial State	Standard Deviation Value
Position	20 m
Velocity	0.01 m/s
Clock bias	14 m
Clock drift	20 m/s

Dynamics Model. The dynamics matrix **F** describes the motion of the satellite, and is generated using the same equations as the truth generation. The Kalman filter **F** matrix includes the clock terms, making it a 10 × 10 matrix. The initial covariance matrix **P** describes the accuracy of the state vector, and will be updated as the filter iterates. The process noise covariance matrix **Q** describes the errors associated with propagating the state covariance matrix **P** through time. The **Q** matrix includes the process noise value of the GEO satellite and the related clock q values. The **Q** matrix is equal to the **Q** matrix used in the truth generation and the clock q values are taken from Table 1, depending upon the type of clocks that are used. (The only difference is that the clock and position/velocity estimation are all done simultaneously.) The **Q** matrix used in the Kalman filter does not change throughout the simulation. Standard Kalman filter propagation equations were applied within the simulation **[6]**.

Measurement Model. The measurement model used in the simulation is

$$\mathbf{z}(t_i) = \mathbf{h}\left[\mathbf{x}(t_i), t_i\right] + \mathbf{v}(t_i) \tag{13}$$

where

$\mathbf{z}(t_i)$ = measurement vector at time t_i

$\mathbf{v}(t_i)$ = zero-mean white Gaussian measurement noise of strength $\mathbf{R} = \mathrm{E}[\mathbf{v}^{\mathrm{T}}(t_i)\,\mathbf{v}(t_i)]$

and, for GPS measurements

$$\mathbf{h}\left[\mathbf{x}(t_i), t_i\right] = \sqrt{(x^{sat} - x_{rec})^2 + (y^{sat} - y_{rec})^2 + (z^{sat} - z_{rec})^2} + c\delta t_{rec} - c\delta t^{sat} \tag{14}$$

The measurement equation for the TWTT measurements was given in Equation (11).

After the **h** vector equations are written, the measurement partial derivative matrix **H** is constructed. The **H** matrix relates the linearized observations to the estimated states, and is expressed for n measurements as:

$$\mathbf{H} = \begin{bmatrix} H_1 \\ H_2 \\ \vdots \\ H_n \end{bmatrix} \tag{15}$$

where

$$H_1 = \frac{\delta h_1(\hat{\mathbf{x}})}{\delta \hat{\mathbf{x}}}, H_2 = \frac{\delta h_2(\hat{\mathbf{x}})}{\delta \hat{\mathbf{x}}}, \cdots, H_n = \frac{\delta h_n(\hat{\mathbf{x}})}{\delta \hat{\mathbf{x}}} \tag{16}$$

$$\frac{\delta h_1(\hat{\mathbf{x}})}{\delta \hat{\mathbf{x}}} = \begin{bmatrix} \dfrac{\delta h_1(\hat{\mathbf{x}})}{\delta x_1} & \dfrac{\delta h_1(\hat{\mathbf{x}})}{\delta x_2} & \cdots & \dfrac{\delta h_1(\hat{\mathbf{x}})}{\delta x_m} \end{bmatrix} \tag{17}$$

The **H** matrix is of size n by m, where n is the number of measurements and m is the number of states. (In this simulation, m = 10). For example, if there are two pseudorange measurements and one TWTT measurement at a given epoch, the **H** matrix and measurement vector **z** will be:

$$\mathbf{H} = \begin{bmatrix} \mathbf{e}_x^1 & \mathbf{e}_y^1 & \mathbf{e}_z^1 & 0 & 0 & 0 & 1 & 0 & 0 & 0 \\ \mathbf{e}_x^2 & \mathbf{e}_y^2 & \mathbf{e}_z^2 & 0 & 0 & 0 & 1 & 0 & 0 & 0 \\ 0 & 0 & 0 & 0 & 0 & 0 & 1 & 0 & -1 & 0 \end{bmatrix} \tag{18}$$

$$\mathbf{z} = \begin{bmatrix} \rho_1 \\ \rho_2 \\ TWTT \end{bmatrix} \tag{19}$$

where

$$\mathbf{e}_x = \frac{x_{rec} - x^{sat}}{\sqrt{(x^{sat} - x_{rec})^2 + (y^{sat} - y_{rec})^2 + (z^{sat} - z_{rec})^2}}$$

$$\mathbf{e}_y = \frac{y_{rec} - y^{sat}}{\sqrt{(x^{sat} - x_{rec})^2 + (y^{sat} - y_{rec})^2 + (z^{sat} - z_{rec})^2}}$$

$$\mathbf{e}_z = \frac{z_{rec} - z^{sat}}{\sqrt{(x^{sat} - x_{rec})^2 + (y^{sat} - y_{rec})^2 + (z^{sat} - z_{rec})^2}}$$

In the example given above, the corresponding **R** matrix is:

$$\mathbf{R} = \begin{bmatrix} \sigma_{PR1}^2 & 0 & 0 \\ 0 & \sigma_{PR2}^2 & 0 \\ 0 & 0 & \sigma_{TWTT}^2 \end{bmatrix} \tag{20}$$

where

σ_{PR} = standard deviation value of pseudorange measurement noise

σ_{TWTT} = standard deviation value of TWTT measurement noise.

Standard extended Kalman filter measurement incorporation equations were implemented within the *kalman* function of the simulation. More details on the Kalman filter implementation can be found in **[13]**.

RESULTS

Analyzing the simulation results involves comparing the Kalman filter estimated state with the true state. The analysis depends on the simulation type, being either a single run or a Monte Carlo collection of runs. All internal calculations within the simulator were performed in the ECI frame. However, prior to interpreting the results, the errors were all converted to ECEF coordinates, so that they would be easier to interpret. This is mostly due to the fact that the GEO satellite is nearly stationary in ECEF coordinates.

The most important result is the three-dimensional positioning error, which will be expressed as Mean Radial Spherical Error (MRSE). The MRSE is analogous to a three-dimensional Distance Root Mean Square (DRMS) value. For a Monte Carlo simulation, the MRSE for a particular epoch is calculated by using the following equation:

$$MRSE = \sqrt{\frac{\sum_{i=1}^{n}\left(x_i^2 + y_i^2 + z_i^2\right)}{n}} \tag{21}$$

where

n = number of simulation runs
$x_i = X_i^{true} - X_i^{filter}$ = difference of truth and filter X position for epoch i
$y_i = Y_i^{true} - Y_i^{filter}$ = difference of truth and filter Y position for epoch i
$z_i = Z_i^{true} - Z_i^{filter}$ = difference of truth and filter Z position for epoch i.

The MRSE value can also be calculated by using the standard deviation values that exist in the covariance matrix for a particular epoch, as seen below.

$$MRSE = \sqrt{\frac{\sum_{i=1}^{n}\left(x_i^2 + y_i^2 + z_i^2\right)}{n}} \approx \sqrt{\sigma_x^2 + \sigma_y^2 + \sigma_z^2} \tag{22}$$

where

$\sigma_x, \sigma_y, \sigma_z$ = standard deviation values for the X, Y, Z coordinates.

Using a Monte Carlo simulation, each run will generate different position values, but the filter-computed covariance values will be the same for every single run. As a result, the covariance standard deviation values from a single run can replace the position values from hundreds of runs in a Monte Carlo simulation, if the filter modeling is accurate.

After the MRSE is calculated for each time epoch, the Root Mean Square (RMS) is calculated for the entire collection of epochs, using Equation (23). The final result is a single RMS value that depicts the level of error in the estimated GEO satellite position.

$$RMS = \sqrt{\frac{\sum_{i=1}^{n} MRSE_i^2}{n}} \tag{23}$$

where

n = number of epochs
$MRSE_i$ = MRSE for epoch i.

COVARIANCE ANALYSIS VALIDATION

As a first step in validating the simulation model, several Monte Carlo simulations were performed to analyze the statistical results and confirm the output was reasonable. The Monte Carlo simulations consisted of 100 iterations. Each simulation uses the same parameters, but uses a different set of random numbers produced by the random number generator in MATLAB®. Figure 7 shows the estimation error in the Y direction for 100 Monte Carlo runs using a "standard" stand-alone GPS receiver (i.e., no TWTT

measurements). The areas of error growth occur when there are very few GPS measurements available. For this simulation, the GEO was placed over 0° latitude and 0° longitude, so the Y direction represents the local vertical direction.

The Monte Carlo ensemble mean and standard deviation are shown in Figure 8, along with the filter-computed standard deviation for the same runs. Note that the filter does a good job of capturing the ensemble results. Other scenarios were run with similar correspondence between the filter-computed values and the Monte Carlo values. Monte Carlo simulations that include TWTT measurements had similar performance as the non-TWTT case. Based upon this performance, the filter-computed values were deemed to be sufficient to characterize the simulation output. By doing so, results were able to be obtained by performing a single run of the filter for any given scenario.

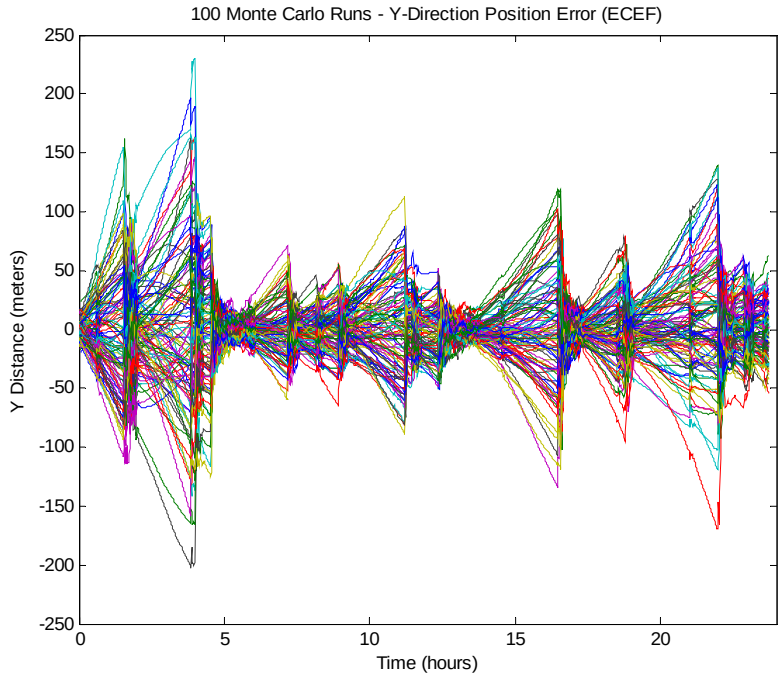

Figure 7. 100 Monte Carlo runs, standard receiver, ovenized crystal oscillator, no TWTT measurements.

SCENARIO DESCRIPTIONS

There were five basic scenarios that were simulated:

1. *Crystal GEO, no TWTT.* This scenario is considered the current performance baseline, as it represents the case where the solution is based entirely on a single GPS receiver in orbit on the GEO satellite with a good-quality ovenized crystal (non-atomic) clock, and no use of TWTT measurements.
2. *Rb GEO, no TWTT.* The only difference between this scenario and Scenario 1 is that the GPS receiver in orbit is now driven by a rubidium clock in the GEO satellite. There is still no TWTT involved.
3. *Crystal GEO, Rb TWTT.* In this case, the GEO satellite has an ovenized crystal clock, but a TWTT system is used to measure the difference between the onboard clock and a rubidium clock

that is on the ground. (TWTT 1-σ accuracy = 0.3m ≈ 1ns). This TWTT measurement is then incorporated as described in Equations (18)-(20), which essentially has the effect of correcting the onboard clock to match the ground-based rubidium clock.

4. *Rb GEO, Rb TWTT.* In this scenario, there is *both* a rubidium clock onboard the GEO satellite, *and* a TWTT system is used to measure the difference between the onboard oscillator and a rubidium clock on the ground.
5. *Crystal GEO, GPS Time TWTT.* In this final scenario, the GEO satellite has an ovenized crystal clock, and a TWTT system is used to measure the difference between the onboard clock and clock on the ground that is slaved to GPS system time.

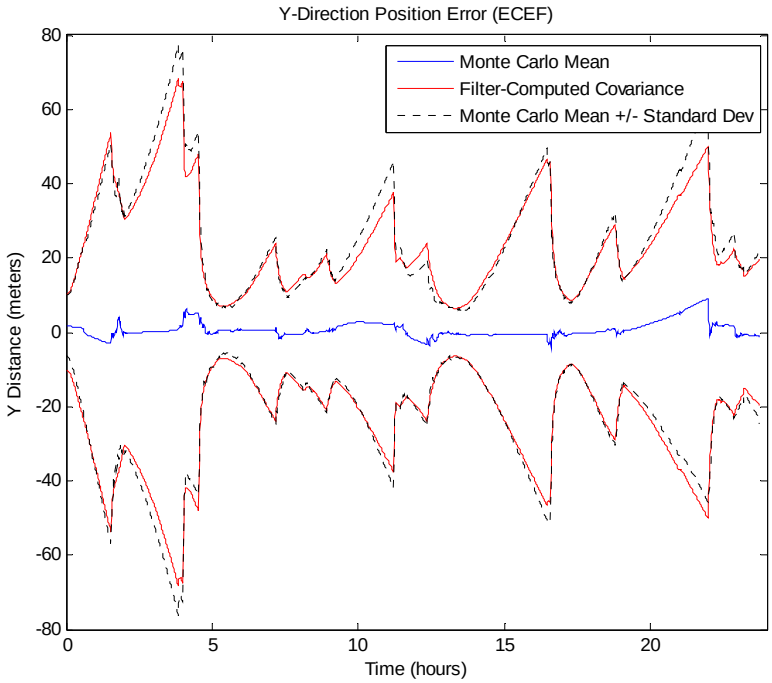

Figure 8. Comparison between Monte Carlo ensemble statistics and filter-computed statistics, standard receiver, ovenized crystal oscillator, no TWTT measurements.

SIMULATION RESULTS

Each of these scenarios was run for each of the six levels of receiver sensitivity described previously, using a TWTT measurement accuracy of 1ns (1σ). Figure 9 shows the entire-run RMS values for each of these test cases (calculated as shown in Equation 23). There are several things to note about the results shown on this plot.

First of all, there is a modest performance improvement when an atomic clock is used rather than a crystal oscillator. Interestingly, the performance was almost identical among Scenarios 2, 3, and 4—all scenarios that include an atomic clock. This would imply that using a TWTT system to synchronize to an atomic clock on the ground would give equivalent navigation performance to placing an atomic clock in orbit. From a practical point of view, this would alleviate the need to place atomic clocks in orbit for many satellite navigation applications.

Secondly, and probably most importantly, there is a drastic performance improvement when the TWTT system is used to synchronize with a ground clock slaved to GPS system time (Case 5). The overall improvement in positioning performance varies between 60%-70% across all receiver models. In essence, this approach is able to measure the absolute error in the GEO GPS receiver clock. As a result, each GPS pseudorange measurement actually becomes a true range measurement. (The GPS pseudorange measurements are called pseudorange measurements rather than range measurements primarily because they include the effects of the receiver clock error.) Note that these effects all happen implicitly within the estimation Kalman filter, as it estimates both the receiver clock error and the GEO satellite position simultaneously, using both GPS pseudorange measurements and TWTT measurements.

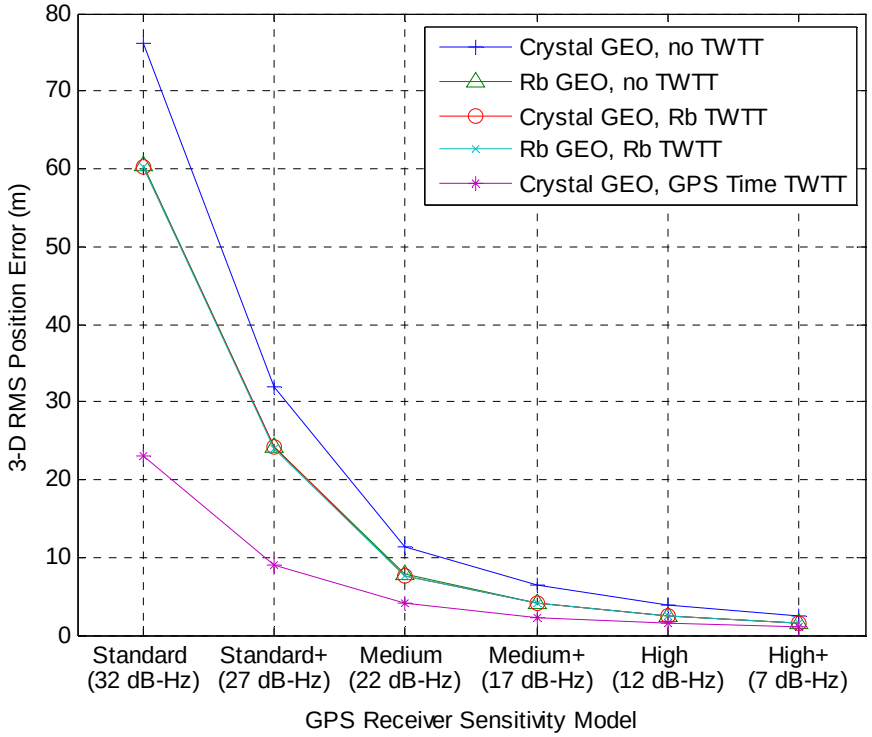

Figure 9. 3D RMS position error vs. GPS receiver sensitivity levels for five basic scenarios.

Finally, it is important to point out that the relative performance improvements (i.e., percentage improvement over Case 1) are similar across all simulated receiver sensitivities. This implies that using TWTT measurements to synchronize with a GPS-disciplined clock is of value in many different situations.

It is insightful to evaluate the results on an axis-by-axis basis. Figure 10 shows the RMS 1-σ errors for both Scenario 1 (no TWTT) and Scenario 5 (TWTT to GPS-synchronized ground clock) on an axis-by-axis basis. The solid lines represent Scenario 1, and the dashed lines represent Scenario 5. It is clear from this plot that the most significant benefit of using the TWTT measurement is observed in the X (vertical) direction. There is a noticeable improvement in the Y and Z directions, particularly for the less sensitive receivers, but in all cases it is the X direction where the largest improvement can be seen. This is consistent with the generally understood principle from GPS that the receiver clock error has the

greatest impact in the vertical direction. It makes sense that using a TWTT system to help estimate receiver clock error would reduce this effect.

ADDITIONAL TESTS

Variation of Ephemeris Date. To ensure the simulation does not depend upon the ephemeris data for a specific day, 9 additional days were selected for comparison. One day was selected out of each year from 1997 to 2006, providing a comprehensive evaluation pool. Each simulation was identical, other than the different ephemeris date, and used the worst-case scenario of a standard sensitivity receiver with no TWTT measurements. While the absolute 3-D RMS error magnitudes did show minor variations between different ephemeris sets (up to 17% difference), the overall trends observed in Figure 10 were nearly equivalent for all ephemeris sets. It is apparent that differing ephemeris dates do not have a significant impact on the results of the simulation.

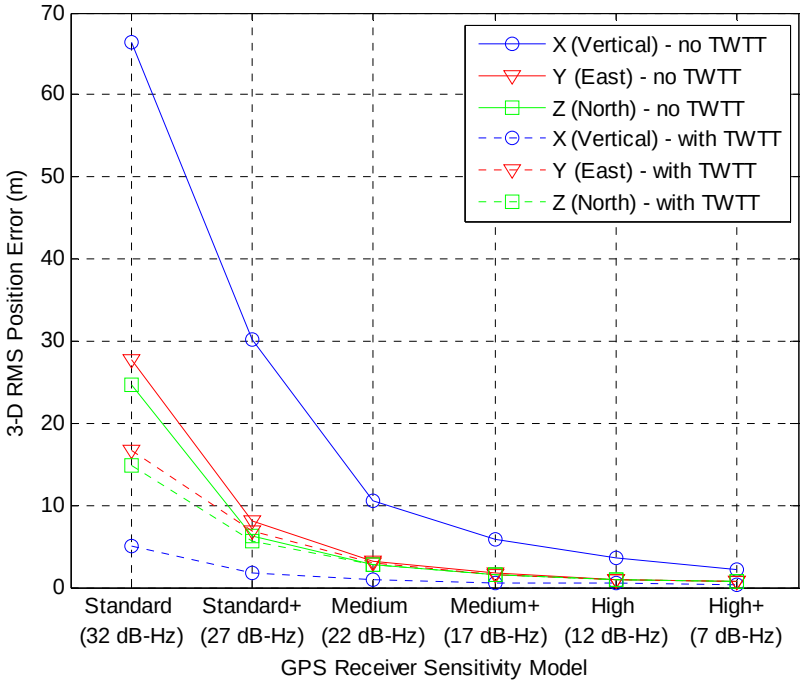

Figure 10. Axis-by-axis evaluation of results for Scenarios 1 and 5.

Required accuracy of GPS time synchronization for Scenario 5. In Scenario 5, the TWTT measurement is taken relative to a clock on the ground that is slaved to GPS system time. Inherently, there will be errors in this measurement due to both TWTT measurement accuracy and errors in the GPS-slaved clock on the ground (i.e., the difference between the reference clock and true GPS time). Both of these types of errors will have the same effect on the results, so they are considered to be lumped together as a total TWTT measurement error for the Scenario 5 cases.

In order to evaluate the sensitivity of the results to this total TWTT measurement error, the Scenario 5 results were recalculated for a range of TWTT measurement error values between 0.3 ns and 100 ns, and the results are shown in Figure 11 (along with the baseline case with no TWTT measurements, for comparison purposes). It is interesting to note that the simulated results are not highly dependent upon

TWTT measurement accuracy, and that significant degradations in performance are not seen until the worst case value of 100 ns.

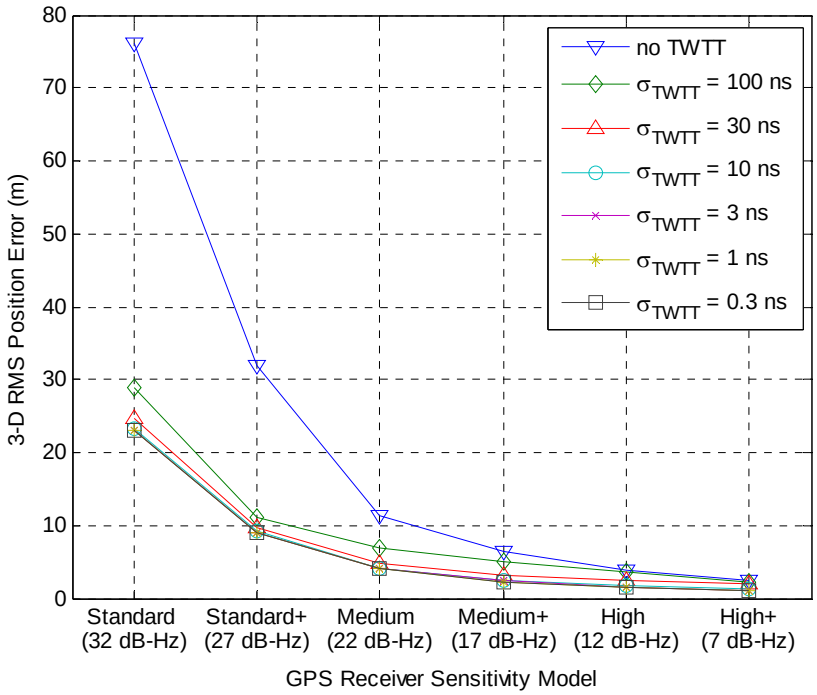

Figure 11. 3-D RMS position error for varying TWTT measurement errors for Scenario 5 (TWTT with reference clock synchronized with GPS Time).

It should be noted that all errors in this simulation were modeled as white, Gaussian errors, and that if there were time-correlated errors, the solutions would be biased and not be as good as the simulation predicts. (By its very nature, the covariance analysis assumes an unbiased solution). Of course, the level of measurement error correlation depends upon the frequency at which measurements are incorporated.

CONCLUSIONS

This simulation demonstrated that TWTT measurements can be extremely useful in improving the positioning performance of high-altitude satellites. The largest benefit comes from using TWTT measurements to synchronize between the GPS receiver clock at GEO and a clock on the ground slaved to GPS system time. In this case, 3-D RMS positioning accuracy was improved between 60%-70%. The level measurement error of the TWTT measurement was not critical to the results for this simulation as long as the error was below 30 ns. Also, the greatest positioning improvement is observed in the vertical direction.

A more modest, but still significant (21%-38%), performance improvement was obtained when TWTT was used to synchronize between the GPS receiver at GEO and an atomic clock on the ground. It was shown that the performance in this case was equivalent to the performance of placing at atomic clock in orbit.

Use of TWTT measurements allows any standard GPS receiver to operate effectively on a GEO satellite with reasonable accuracy. Accurate GPS navigation in high-altitude orbits provides numerous opportunities, such as automated station-keeping in a GEO orbit. Also, by substituting automation and removing the ground-based ranging systems, the cost reduction incurred by reducing ground support is considerable.

DISCLAIMER

The views expressed in this paper are those of the authors and do not reflect the official policy or position of the United States Air Force, Department of Defense, or the U.S. Government.

REFERENCES

[1] R. Beckman, T. Celano, S. Francis, A. Gifford, P. Howe, and J. Warriner, 2003, *"Dynamic Two-Way Time Transfer to Moving Platforms,"* in Proceedings oft the IEEE International Frequency Control Symposium and PDA Exhibition Jointly with the 17th European Frequency and Time Forum (EFTF), 4-8 May 2003, Tampa, Florida, USA (IEEE Publication 03CH37409), pp. 266-272.

[2] T. Celano, J. Warriner, S. Francis, A. Gifford, P. Howe, and R. Beckman. 2003, *"Two-Way Time Transfer to Airborne Platforms Using Commercial Satellite Modems,"* in Proceedings of 34th Annual Precise Time and Time Interval (PTTI) Systems and Applications Meeting, 3-5 December 2002, Reston, Virginia, USA (U.S. Naval Observatory, Washington, D.C.), pp. 353-366.

[3] K. Cook, J. Raquet, and R. Beckman, 2006, *"Characterizing the Impact of Incorporating Two-Way Time Transfer Measurements on Network Differential GPS Position Solutions*," in Proceedings of the ION GNSS 2006 Meeting, 26-29 September 2006, Fort Worth, Texas, USA (Institute of Navigation, Alexandria, Virginia), pp. 822-833.

[4] P. Hwang, G. McGraw, B. Schnaufer, and D. Anderson, 2005, *"Improving DGPS Accuracy With Clock Aiding Over Communication Links,"* in Proceedings of the ION GNSS 2005 Meeting, 13-16 September 2005, Long Beach, California, USA (Institute of Navigation, Alexandria, Virginia), pp. 1961-1970.

[5] D. Hanson, 1989, *"Fundamentals of Two-Way Time Transfers by Satellite,"* in Proceedings of the 43rd Annual Frequency Control Symposium, 1989, Boulder, Colorado, USA (IEEE Publication 89CH2690-6), pp. 174-178.

[6] R. G. Brown and P. Y. C. Hwang. 1997, **Introduction to Random Signals and Applied Kalman Filtering** (John Wiley & Sons, New York).

[7] S. Hutsell, 1995, *"Fine Tuning GPS Clock Estimation in the MCS,"* in Proceedings of the 26th Annual Precise Time and Time Interval (PTTI) Applications and Planning Meeting, 6-8 December 1994, Reston, Virginia, USA (NASA Conference Publication 3302), pp. 63-74 (see Errata Vol. 2).

[8] P. Misra and P. Enge, 2001, **Global Positioning System: Signals, Measurements, and Performance** (Ganga-Jamuna Press, Lincoln, Massachusetts).

[9] F. Czopek and S. Shollenberger, 1993, *"Description and Performance of the GPS Block I and II L-Band Antenna and Link Budget,"* in Proceedings of the ION GPS 1993 Meeting, 22-24 September 1993, Salt Lake City, Utah, USA (Institute of Navigation, Alexandria, Virginia), pp. 37-43.

[10] T. Powell, P. Martzen, S. Sedlacek, C. Chao, R. Silva, A. Brown, and G. Belle, 1999, *"GPS Signals in a Geosynchronous Transfer Orbit: 'Falcon Gold' Data Processing,"* in Proceedings of the 1999 National Technical Meeting of the Institute of Navigation, 25-27 January 1999, San Diego, California, USA (Institute of Navigation, Alexandria, Virginia), pp. 575-586.

[11] C. Frey and J. Ruiz, 2005, *"Geosynchronous Satellite Use of GPS,"* in Proceedings of the ION GNSS-2005, 13-16 September 2005, Long Beach, California, USA (Institute of Navigation, Alexandria, Virginia), pp. 1227-1232.

[12] A. Brown and K. Gold, *"Architecture and Performance Testing of a Software GPS Receiver for Space-based Applications,"* in Proceedings of the IEEE Aerospace Conference, 6-13 March 2004, Big Sky, Montana, USA, pp. 2404-2416.

[13] B. Dainty, 2007, "*Use of Two-Way Time Transfer Measurements to Improve Geostationary Satellite Navigation,"* MS thesis, Air Force Institute of Technology, Wright-Patterson AFB, Ohio, USA.